SCIENTIFIC REPORTS

OPEN

SUBJECT AREAS:
CHEMICAL ENGINEERING
SOLAR CELLS

Received
10 April 2014

Accepted
6 June 2014

Published
1 July 2014

Correspondence and requests for materials should be addressed to D.L. (daeyeon@seas.upenn.edu) or J.H.K. (jonghak@yonsei.ac.kr)

Mesoporous TiO_2 Bragg Stack Templated by Graft Copolymer for Dye-sensitized Solar Cells

Jung Tae Park[1,2], Won Seok Chi[1], Sang Jin Kim[1], Daeyeon Lee[2] & Jong Hak Kim[1]

[1]Department of Chemical and Biomolecular Engineering, Yonsei University, 262 Seongsanno, Seodaemun-gu, Seoul 120-749, South Korea, [2]Department of Chemical and Biomolecular Engineering, University of Pennsylvania, 220 South 33rd Street, Philadelphia, Pennsylvania 19104, USA.

Organized mesoporous TiO_2 Bragg stacks (om-TiO_2 BS) consisting of alternating high and low refractive index organized mesoporous TiO_2 (om-TiO_2) films were prepared to enhance dye loading, light harvesting, electron transport, and electrolyte pore-infiltration in dye-sensitized solar cells (DSSCs). The om-TiO_2 films were synthesized via a sol-gel reaction using amphiphilic graft copolymers consisting of poly(vinyl chloride) backbones and poly(oxyethylene methacrylate) side chains, *i.e.*, PVC-*g*-POEM as templates. To generate high and low index films, the refractive index of om-TiO_2 film was tuned by controlling the grafting ratio of PVC-*g*-POEM *via* atomic transfer radical polymerization (ATRP). A polymerized ionic liquid (PIL)-based DSSC fabricated with a 1.2-μm-thick om-TiO_2 BS-based photoanode exhibited an efficiency of 4.3%, which is much higher than that of conventional DSSCs with a nanocrystalline TiO_2 layer (nc-TiO_2 layer) (1.7%). A PIL-based DSSC with a heterostructured photoanode consisting of 400-nm-thick organized mesoporous TiO_2 interfacial (om-TiO_2 IF) layer, 7-μm-thick nc-TiO_2, and 1.2-μm-thick om-TiO_2 BS as the bottom, middle and top layers, respectively, exhibited an excellent efficiency of 7.5%, which is much higher than that of nanocrystaline TiO_2 photoanode (3.5%).

Since Gratzel's breakthrough discovery in 1991, dye-sensitized solar cells (DSSCs) have received great attention as promising alternatives to traditional silicon-based photovoltaic devices. These DSSCs are especially attractive because of their high power conversion efficiency, low cost, and facile eco-friendly fabrication[1]. A standard DSSC consists of a wide band gap semiconductor nanocrystalline film deposited on a fluorine-doped tin oxide (FTO) glass as the photoanode, a photosensitizer (dye), a platinum-coated FTO glass as the counter electrode, and a liquid redox electrolyte typically based on an iodide/triiodide (I^-/I_3^-) redox couple in an organic solvent. Although high photovoltaic conversion efficiencies have been reported, these DSSCs typically utilize liquid electrolytes as a redox mediator[2–7], which presents serious limitations such as leakage and iodine (I_2) corrosion and consequently impedes the practical applications of these devices. Significant efforts to replace liquid electrolytes with solid materials have been devoted; examples include quasi-solid or solid polymers[8,9], conducting polymers[10–13] and organic ionic plastic crystal electrolytes[14,15]. In addition, there has been active progress in recent years in fabricating high efficiency solid/quasi-solid DSSCs with perovskites[16–18]. In addition to these developments involving solid-state electrolytes, further improvements in the design of mesoporous TiO_2 photoanode could potentially lead to highly efficient solid/quasi-solid DSSCs. In this regard, well-organized mesoporous TiO_2 that our group has developed represents an excellent photoanode material because of its inherent high porosity, ordered pores, and interconnectivity[19].

In addition to using organized mesoporous TiO_2 photoanode, an additional method to enhance the performance of DSSCs is to enhance the light harvesting by incorporating photonic structures into the devices. For example, one-dimensional photonic crystals, such as Bragg stacks (BS), have been applied to liquid-based and solid-state DSSCs to enhance their light harvesting properties and in turn the power conversion efficiency[20–24]. In previous reports, BS were prepared directly on top of the photoanode or positioned behind the counter electrode so that light transmitted through the photoanode would be reflected back into the electrode, which in turn improves the likelihood of successful harvesting[20–24].

SiO_2 and TiO_2 constitute the most common pair of nanomaterials used to achieve high quality BS layers because they have large refractive index contrast (SiO_2; 1.45, TiO_2; 2.44) and can be prepared simply from liquid phases by spin or dip coating[25,26]. However, the use of BS structures based on SiO_2/TiO_2 pairs in the DSSC

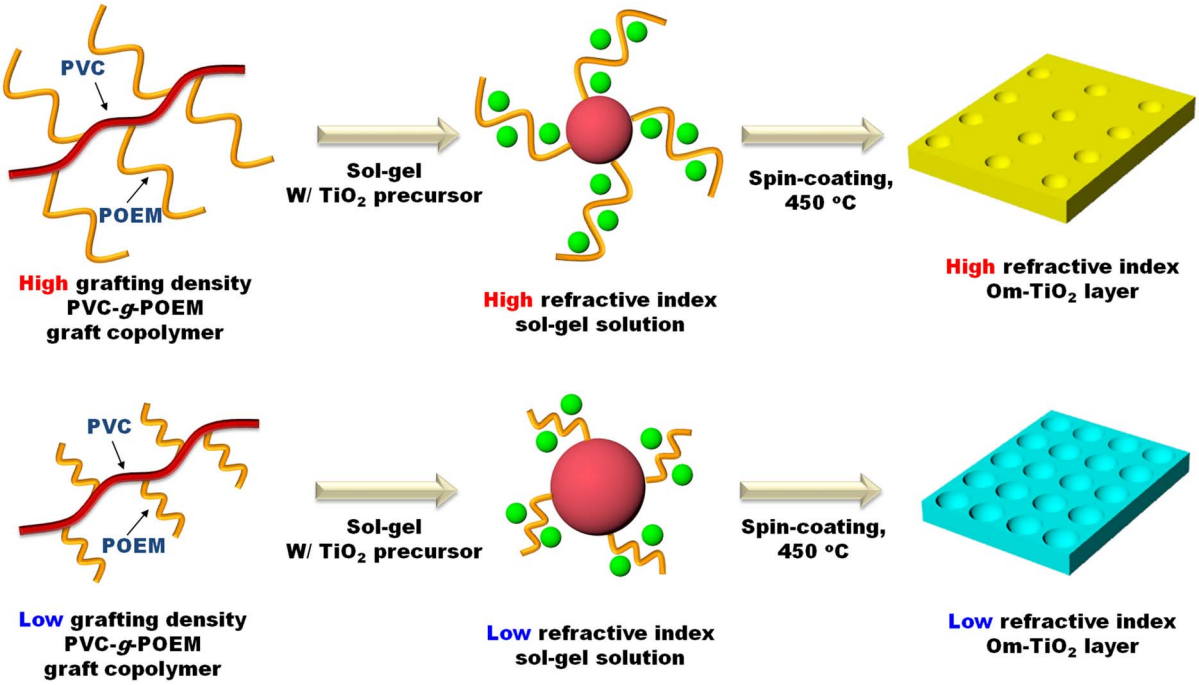

Figure 1 | Schematic representation of the preparation route for the om-TiO_2 layer using PVC-*g*-POEM graft copolymers.

applications has some limitations in achieving high cell performance because of increased charge recombination in the non-conducting SiO_2 layers. The increased charge recombination results in a significant reduction in the open circuit photovoltage (V_{oc}). Furthermore, the penetration of polymeric electrolytes into photoanode through the BS presents an additional challenge. Incomplete pore filling by the electrolyte inhibits sufficient interfacial contact between the photoanode and the electrolyte, and results in poor photovoltaic performance. An ideal BS structure would constitute TiO_2 for both the high and low index layers. Although, refractive index-tunable TiO_2 layers have been used as building blocks to prepare all-TiO_2 BS and these structures showed interesting photoconductivity and optical properties, its solar cell application has not been presented yet[27,28].

In this report, we present the fabrication of an organized mesoporous TiO_2 Bragg stack (om-TiO_2 BS) for use as a photoanode in DSSCs to improve power conversion efficiency. The combination of the reflective property and the high surface area makes these om-TiO_2 BS ideal candidates for photoanode applications in DSSCs with excellent electron transport and electrolyte infiltration properties. An om-TiO_2 BS, which comprises of high (2.0) and low (1.7) refractive index om-TiO_2 layers, is prepared *via* a sol-gel process using two copolymer templates with different graft ratios. The enhancement in the light harvesting properties and electrochemical performance of DSSCs through the incorporation of the om-TiO_2 BS was characterized by scanning electron microscopy (SEM), UV-Vis spectroscopy, incident photon-to-electron conversion efficiency (IPCE), electrochemical impedance spectroscopy (EIS), and intensity modulated photocurrent/voltage spectroscopy (IMPS/IMVS). We discuss the underlying mechanism behind the device performance improvement based on these results. To our best knowledge, our work is the first report describing the use of all om-TiO_2 BS as a photoanode in DSSCs.

Result and Discussion

An om-TiO_2 BS reflector was prepared by alternate casting of a high refractive index om-TiO_2 layer and a low refractive index om-TiO_2 layer. The two types of om-TiO_2 layers of different porosity were deposited on FTO glass *via* alternating spin coating (Figure 1). The refractive index of each om-TiO_2 layer was controlled by using PVC-*g*-POEM graft copolymers with different grafting density, which were synthesized *via* the atomic transfer radical polymerization (ATRP) method[29,30]. When PVC-g-POEM graft copolymers and a titanium precursor, titanium(IV) isopropoxide (TTIP), are combined, the hydrophilic TTIP selectively incorporates in the hydrophilic domains of POEM. TiO_2 crystallites are formed *in situ* during calcination confined to the POEM domains, while the mesopores are produced upon the removal of the hydrophobic PVC domains. The average pore size of om-TiO_2 films prepared with a high grafting density copolymer (weight ratios of PVC : POEM were 1 : 6, referred to as type1) was approximately 30 nm, whereas that of om-TiO_2 films templated with a low grafting density copolymer (weight ratios of PVC : POEM were 1 : 1.5, referred to as type2) was 70 nm. Also, the porosity of om-TiO_2 films prepared with the high grafting density copolymer was lower than that of those with the low grafting density copolymer, as shown in Figure 2.

The position of a Bragg diffraction peak, which is directly related to the optical properties and structure of the reflector, is determined by the refractive index and thickness of each om-TiO_2 layer in the om-TiO_2 BS. The position of the Bragg reflection peak was calculated using the following equation (1). The central wavelength of the Bragg reflection of order m is

$$m\lambda_B = 2(n_1 d_1 + n_2 d_2) \quad (1)$$

where m is diffraction order, n_i is the refractive index of each layer, and the d_i is the thickness of each layer[31]. In addition, the refractive index is directly correlated with porosity. If each layer is assumed to be composed of anatase phase, porosity can be calculated using the following equation (2):

$$\text{Porosity} = 1 - (n^2 - 1)/(n_0^2 - 1) \quad (2)$$

where n is the refractive index of each om-TiO_2 layer and n_0 is the refractive index of the pure anatase TiO_2 layer[32]. Using ellipsometry, the refractive index, thickness, and porosity of the high refractive index om-TiO_2 layers were determined to be 2.0 ± 0.05, 125 ± 5 nm, and 0.38 ± 0.02, respectively. The corresponding values for the low refractive index om-TiO_2 layer were 1.7 ± 0.05, 130 ± 5 nm,

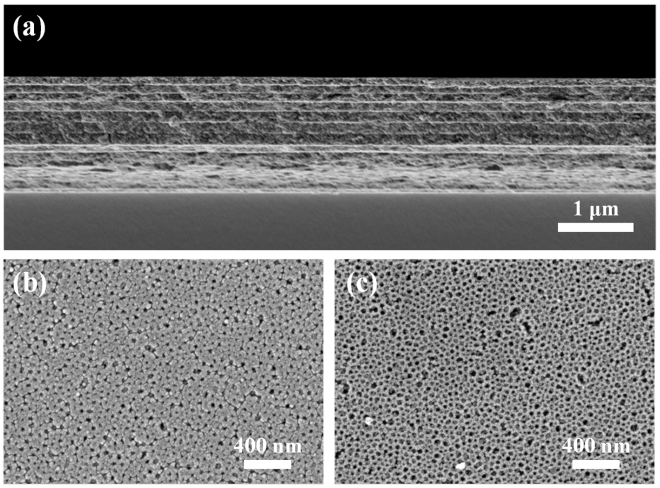

Figure 2 | FE-SEM image of om-TiO_2 BS consisting of nine alternating layers of high refractive index om-TiO_2 and low refractive index om-TiO_2, (a) cross-section of om-TiO_2 BS on FTO glass, (b) plane-view of high refractive index om-TiO_2 layer derived from type 1 (PVC-*g*-POEM with high grafting degree), and (c) plane-view of low refractive index om-TiO_2 layer derived from type 2 (PVC-*g*-POEM with low grafting degree). Cross-section of the om-TiO_2 BS was obtained by fracturing FTO glass.

and 0.62 ± 0.02, respectively. The fabricated om-TiO_2 BS was adjusted to have one of the higher order reflectance peaks at approximately 480 nm.

Figure 2(a) shows a cross sectional FE-SEM image of the om-TiO_2 BS templated by PVC-g-POEM graft copolymers, and Figures 2(b,c) show a plan-view FE-SEM image of high and low refractive index om-TiO_2 layers, respectively. The plan-view FE-SEM images clearly demonstrate that porosity and pore size distribution (refractive index) of each om-TiO_2 layer can be controlled using the two graft copolymer templates with different grafting density. The cross sectional FE-SEM image confirms the long range order and crack-free structure of the high and low refractive index om-TiO_2 layers used to generate the BS reflector. Although spin-coating conditions were identical for each om-TiO_2 layer, the first layer deposited on the FTO glass was thicker than the subsequently deposited om-TiO_2 layer likely due to the different surface wetting properties of the FTO glass and om-TiO_2 layers[33].

The om-TiO_2 BS reflector deposited on FTO glass function as a highly efficient back reflector as well as the dye adsorbable active layer. This combination likely increases the beam path of solar irradiation within the photoanode due to reflection at each interface between high and low-index layers, which we believe improves the light harvesting efficiency of the photoanode. Compared to conventional TiO_2 nanoparticle-based nanocrystalline (nc-TiO_2) layers (D20, Solaronix), the om-TiO_2 BS has a larger specific surface area due to high porosity, which also enhances the amount of dye loading. The surface area of the om-TiO_2 BS prepared with high (84.1 m^2/g) and low (75.3 m^2/g) refractive index om-TiO_2 layers was larger than that that of the photoanode prepared with nc-TiO_2 layers (56.1 m^2/g), as determined using N_2 adsorption-desorption measurements. The om-TiO_2 BS with high porosity is expected to improve electron transport and solid electrolyte infiltration, which eventually would lead to lower charge recombination and enhanced interfacial properties in DSSCs.

Next, we characterized the photonic properties of the om-TiO_2 BS photoanode. An om-TiO_2 BS with high uniformity and quality was fabricated over a large area of at least 2 × 3 cm^2 without striations and cracks, as shown in Figure 3(a). The photonic performance was compared with that of a control cell based on commercial nanocrystalline TiO_2 nanoparticles (nc-TiO_2 cell). The thickness of two types

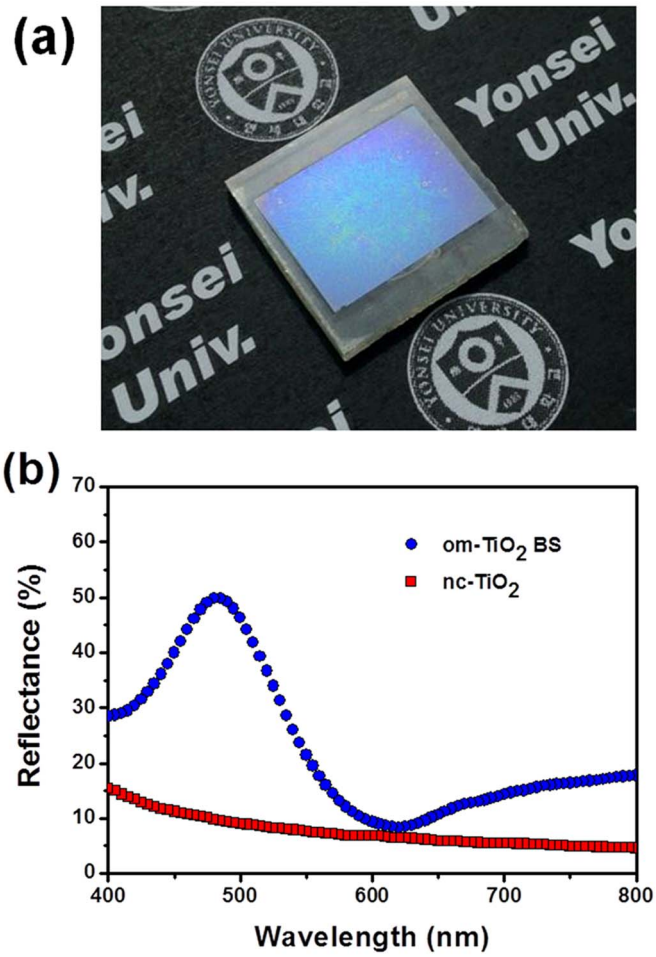

Figure 3 | (a) Photograph of the om-TiO_2 BS, and (b) reflectance spectra obtained from the om-TiO_2 BSand nc-TiO_2 layer before dye adsorption without electrolytes under frontal illumination.

of photoanode was maintained at approximately 1.2 μm, and at least three cells were prepared and tested for comparison. Figure 3 (b) shows the reflectance spectra of the nc-TiO_2 layer and om-TiO_2 Bragg stack. The nc-TiO_2 layer showed low reflectance in the entire visible wavelength region, which indicated that unabsorbed light passed through the nc-TiO_2 layer. However, the om-TiO_2 BS exhibited high reflectance in the entire visible wavelength region, which is a direct consequence of the structure of the om-TiO_2 layers. As expected from the Bragg condition (equation 1), the om-TiO_2 BS has the Bragg reflectance peak around 480 ~ 520 nm, which overlaps with one of the strong absorption peaks of ruthenium N719 dye[23,34]. The maximum reflectance value of om-TiO_2 BS was 50% higher than nc-TiO_2 layer when nine stacks of alternating high and low refractive index om-TiO_2 layers were deposited. Based on these results, it is expected that the beam path of the incident light is extended within the om-TiO_2 BS photoanode, which is expected to improve the light harvesting efficiency of DSSCs.

We tested the device performance of a solid PIL-based DSSC fabricated with the om-TiO_2 BS as the photoanode and compared its light harvesting efficiency to that of a DSSC generated with a nc-TiO_2 layer as its photoanode. Poly((1-(4-ethenylphenyl)methyl)-3-butyl-imidazolium iodide) (PEBII)[19,29] was synthesized *via* free radical polymerization and utilized as the solid electrolyte without any additives. The synthesized PEBII showed high mobility and ionic conductivity (2.0 × 10^{-4} S/cm at 25°C) due to facile ion transport through well-organized structures with π-π stacking interactions and low glass transition temperature (~−4°C). The IPCE measurements

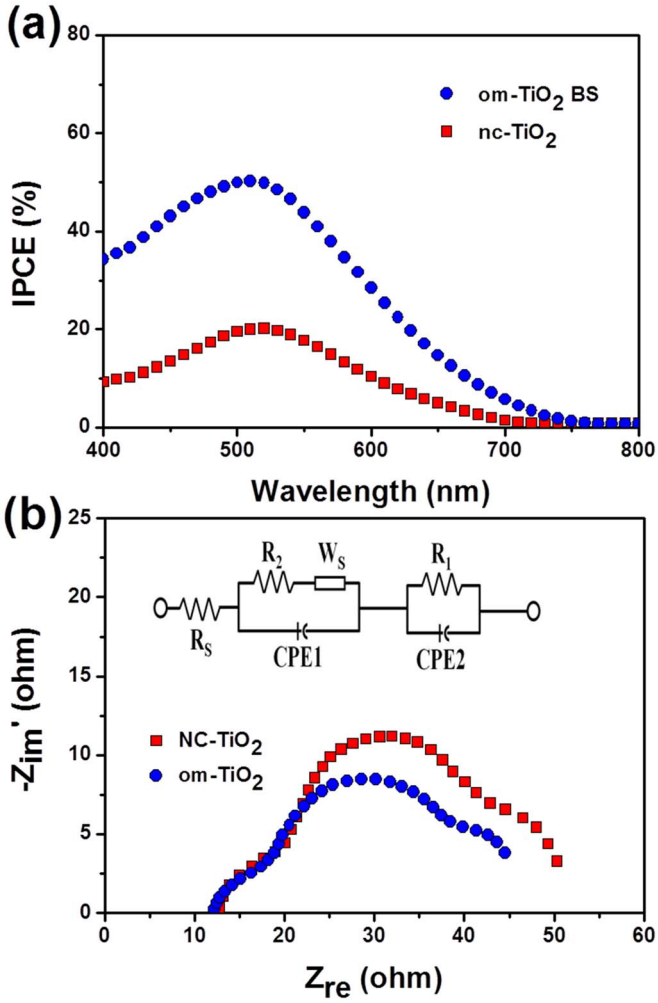

Figure 4 | (a) IPCE curves and (b) Nyquist plots of a solid PIL-based DSSCs fabricated with om-TiO_2 BS and nc-TiO_2 layers measured under an illumination of 100 mW/cm^2. (Inset is equivalent circuit. Details of components are described in the text.).

were performed under normal incident light from the front side as a function of wavelength from 400 nm to 800 nm. The IPCE efficiency (η_{IPCE}) was determined for each device and is closely related to light harvesting efficiency (η_{lh}) through

$$\eta_{IPCE} = \eta_{lh} \cdot \eta_{Inj} \cdot \eta_{col} \quad (6)$$

where η_{Inj} is electron injection efficiency and η_{col} is electron collection efficiency[24]. Figure 4 clearly shows that DSSCs based on the om-TiO_2 BS have significantly higher IPCE over the entire spectrum compared to the nc-TiO_2-based DSSCs. The higher light harvesting efficiency resulting from enhanced dye adsorption (high specific surface area) and extended beam path length are the major contributors to the enhanced IPCE in the DSSCs based on the om-TiO_2 BS. In addition, the IPCE spectra in Figure 4a show that maximum efficiency is located at approximately 520–540 nm, which corresponds to the absorption peak of the N719 ruthenium dye. We also believe that using highly interconnected om-TiO_2 BS layers with high porosity and large pores will have positive effects on the electron collection efficiency (η_{col}). Such enhancement will be discussed more in depth in our analyses of recombination resistances (R_{rec}) and electron lifetime (τ_n).

EIS measurements were carried out to demonstrate the effects of om-TiO_2 BS on the performance of DSSCs. Figure 4b shows the EIS Nyquist plots of the DSSCs with om-TiO_2 BS and nc-TiO_2 layers at open circuit under one sun illumination. Internal/interfacial impedances were determined by fitting experimental data with an equivalent circuit (inset image), which consists of an Ohmic series resistance of the substrate (R_S, starting point of the first semicircle in the EIS Nyquist plot), charge transport resistance at the Pt counter electrode (R_1, first semicircle in the EIS Nyquist plot), charge transfer resistance at the TiO_2 photoanode/dye/electrolyte (R_2, second semicircle in the EIS Nyquist plot), Warburg diffusion in the electrolyte (R_3, third semicircle in the EIS Nyquist plot), and constant phase element of capacitance corresponding to R_1 (CPE1) and R_2 (CPE2)[34]. Here, we focused on the second semicircle of the plot to investigate charge transfer characteristics at the TiO_2 photoanode/dye/electrolyte. R_2 values determined from the real component (Z_{re}) of the om-TiO_2 BS-based DSSC (16 Ω) were less than 2/3 of nc-TiO_2 layer-based DSSCs (25 Ω), as shown in Figure 4b. This result likely is because the om-TiO_2 BS has high porosity, large pores, and sufficient interconnectivity to allow pore-infiltration of solid electrolyte. Complete pore filling facilitates efficient ion transport and dye regeneration. The EIS Nyquist result also implies that the incorporation of an om-TiO_2 BS decreased charge transfer resistance at the TiO_2 photoanode/dye/electrolyte, which improves the fill factor (*FF*) value. The mechanism underlying the photovoltaic performance improvement of the om-TiO_2 BS-based DSSCs was further investigated by measuring the recombination resistance (R_{rec}) and electron lifetime (τ_n) of the devices as a function of bias voltage as shown in Figure 5. The product of the recombination resistance and the electron transfer capacitance represents the electron lifetime (τ_n) of the DSSC. Larger recombination resistance and longer electron lifetime were obtained in the om-TiO_2 BS-based DSSCs, indicating suppressed recombination process with more efficient electron transfer. This result is attributed to the high porosity and large pores of the om-TiO_2 BS layer, which was templated by the two PVC-*g*-POEM graft copolymers. In short, the om-TiO_2 BS-based DSSC exhibited efficient electron transport due to the suppression of charge recombination, which in turn improves its V_{oc} compared to the nc-TiO_2 layer based cell[35,36].

The photovoltaic performance of om-TiO_2 BS-based cells with N719 dye and PEBII solid electrolyte was measured under a simulated AM 1.5 G illumination intensity of 100 mW/cm^2, as shown in Figure 6. Table 1 summarizes photovoltaic parameters such as open-circuit voltage (V_{oc}), short-circuit current density (J_{sc}), fill factor (*FF*), light-to-electricity conversion efficiency (η), and amount of dye loading. The Beer-Lambert law was used to determine the amount of ruthenium dye (N719) chemisorbed onto different types of photoanodes[37]. As expected, a large enhancement was attained for J_{sc} and *FF* for the DSSC with om-TiO_2 BS compared to the commercial TiO_2 nanocystal-based cell (nc-TiO_2 photoanode). The V_{oc}, J_{sc}, *FF*, and η of the DSSC using a nc-TiO_2 photoanode were determined to be 0.83 V, 3.8 mA/cm^2, 0.54, and 1.7%, respectively. In contrast, the om-TiO_2 BS photoanode-based DSSC had a V_{oc} of 0.84 V, J_{sc} of 8.2 mA/cm^2, *FF* of 0.62, and η of 4.3% with a 1.2 μm photoanode thickness. The V_{oc} was slightly improved for the om-TiO_2 BS photoanode-based DSSC, which is attributable to its well-organized interconnected structure. This structure results in a more effective electron transport pathway and reduces the possibility of electron trapping for charge recombination. The enhanced J_{sc} for the om-TiO_2 BS photoanode-based DSSC is attributed to improved light harvesting efficiency derived from (1) increased light reflection caused by a periodic Bragg stack structure and (2) better dye adsorption due to high specific surface area. As a result of both contributions, J_{sc} was enhanced up to 115% compared to the control cell. There was also an enhancement in *FF* for the om-TiO_2 BS photoanode-based DSSC, which resulted from the high porosity structure of the photoanode. This structure allowed facile and sufficient penetration of solid state electrolyte into TiO_2 nanopores without affecting cell kinetics.

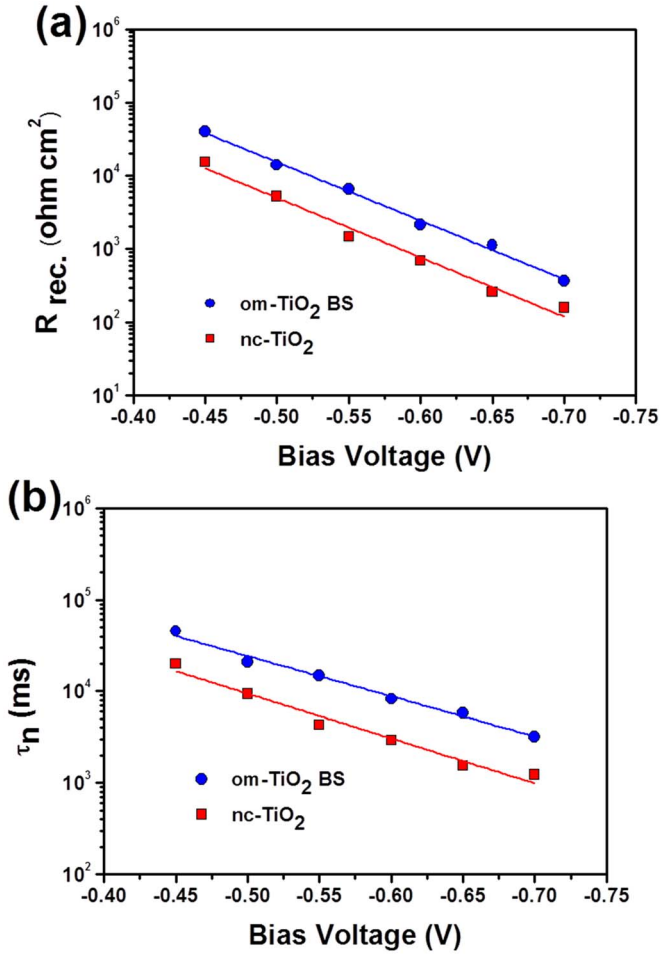

Figure 5 | (b) Diffusion coefficient (D_n), (c) electron lifetime (τ_r), and (d) electron diffusion length (L_n) of a solid PIL-based DSSCs assembled with the om-TiO_2 BS and nc-TiO_2 layer measured by IMPS and IMVS as a function of J_{SC}.

Further enhancements in photovoltaic performance were achieved when the photoanode was prepared with 0.4 μm om-TiO_2 IF, 7 μm NC-TiO_2, and 1.2 μm om-TiO_2 BS as the bottom, middle and top layers, respectively. The om-TiO_2 IF/NC-TiO_2/om-TiO_2 BS photoanode gives the highest light-to-electricity conversion efficiency of 7.5%, which is an increase of 341% compared to the 1.2-μm-thick nc-TiO_2 (1.7%)-based DSSC and 74% compared to the 1.2 μm-om-TiO_2 BS photoanode-based DSSC (4.3%). Also, we note that a DSSC with only a 7-μm-thick nc-TiO_2 photoanode exhibited an energy conversion efficiency of 3.5% (Figure S1, Table S1)[23]. The obtained efficiency of 7.5% is even higher than those obtained from the solid PIL-based DSSCs involving Bragg stacks with TiO_2 and SiO_2 layers as summarized in Table S2[23,24]. The enhanced J_{sc} value obtained with om-TiO_2 IF/nc-TiO_2/om-TiO_2 BS photoanode-based DSSCs is attributed primarily to enhanced light harvesting by TiO_2 films. The increased surface area of om-TiO_2 IF/nc-TiO_2/om-TiO_2 BS photoanode-based DSSCs allows more dye molecules to anchor on the surface of TiO_2 films, leading to better optical absorbance. As shown in Table 1, the amount of dye loading on TiO_2 films was 10.5 nmol/cm^2 for nc-TiO_2, 18.3 nmol/cm^2 for om-TiO_2 BS, and 91.3 nmol/cm^2 for the om-TiO_2 IF/nc-TiO_2/om-TiO_2 BS photoanode. The J_{sc} of the om-TiO_2 IF/nc-TiO_2/om-TiO_2 BS photoanode structure provides approximately 40% enhancement compared to the z highly reflective om-TiO_2 BS layer allows not only reflection as well as scattering of the unabsorbed photons back into the cell but also high dye loading (Figure S1, Table S1), resulting in a noticeable

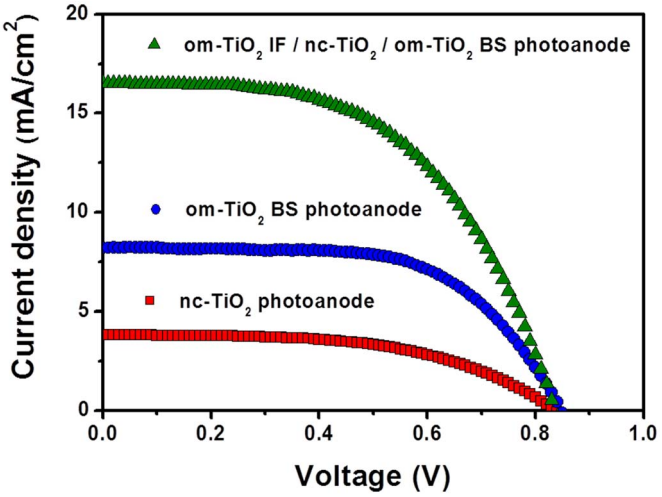

Figure 6 | **Photocurrent density-voltage (*J-V*) curves of a solid PIL-based DSSCs assembled with three kinds of thin TiO_2 photoanodes under conditions of simulated AM 1.5 global solar radiation at 100 mW/cm^2.**

improvement of efficiency. This results in an increase of the photovoltaic light harvesting performance without any adverse effects.

The effectiveness of the om-TiO_2 BS layer can be more clearly demonstrated by characterizing the transmission properties of the ssDSSCs assembled with 7 micron-thick nc-TiO_2 photoanode and the PIL electrolyte (Figure S2). The spectrum clearly shows that rather significant transmission (about 20%) exists between 480 and 520 nm, which is close to one of the absorption peaks of the N719 ruthenium-based dye. This result implies that more than 20% of light is not absorbed by the 7 micron-thick nc-TiO_2 photoanode in the target wavelength region and that the om-TiO_2 reflects unabsorbed photons back to the photoanode. The use of Bragg stacks which have reflection peaks around 480 ~ 520 nm have also been shown to enhance the performance DSSCs by redirecting the unabsorbed photons back to the photoanodes[20,21].

Conclusions

We proposed the use of the om-TiO_2 BS layer, composed of high and low refractive index of om-TiO_2, as a means to improve the not only light harvesting efficiency but also electron transport and electrolyte infiltration in solid-state DSSCs. The om-TiO_2 layers with different refractive indices were prepared *via* a sol-gel process using graft copolymers as templates. Inspired by their multifunctional structure, the om-TiO_2 BS layer based DSSCs (1.2 μm) with solid state electrolyte demonstrate increased light reflection, improved dye loading, reduced charge recombination, and decreased interfacial resistance than DSSCs made with NC TiO_2 layer photoanodes, and consequently high η of 4.3%, a 150% improvement compared to the NC TiO_2 layer-based DSSCs. Moreover, the DSSCs based on the om-TiO_2 IF/NC TiO_2/om-TiO_2 BS heterostructured photoanode shows a η of 7.5% accompanying a V_{oc} of 0.83 V, a J_{sc} of 16.5 mA/cm^2, and a *FF* of 0.55, which is much higher than that of conventional nanocrystaline TiO_2 photoanode (3.5%). This work clearly shows that the BS based on om-TiO_2 layers is a very promising material which has good potential for application in optical sensing, radiation shielding, and energy field.

Methods

Materials. Poly(vinyl chloride) (PVC, M_w = 97,000 g mol^{-1}, M_n = 55,000 g mol^{-1}), poly(oxyethylene methacrylate) (POEM, poly(ethylene glycol) methyl ether methacrylate, M_n = 475 g mol^{-1}), 1,1,4,7,10,10-hexamethyltriethylene tetramine (HMTETA, 99%), copper(I) chloride (CuCl, 99%), titanium(IV) isopropoxide (TTIP, 97%), hydrogen chloride solution (HCl, 37 wt %), sodium hydroxide (NaOH), 1-butylimidazole, 4-chloromethylstyrene, lithium iodide (LiI), magnesium sulfate ($MgSO_4$), 2,2′-azobisisobutyronitrile (AIBN), and chloroplatinic acid hexahydrate

Table 1 | Photovoltaic properties and dye loading values of a solid PIL-based DSSCs fabricated with three kinds of photoanodes at 100 mW/cm² (AM 1.5)

Photoanode	V_{oc} (V)	J_{sc} (mA/cm²)	*FF*	η (%)	Dye loading (nmol/cm²)
nc-TiO_2[a]	0.83	3.8	0.54	1.7	10.5
om-TiO_2 BS[a]	0.84	8.2	0.62	4.3	18.3
om-TiO_2 IF/nc-TiO_2/om-TiO_2 BS[b]	0.83	16.5	0.55	7.5	91.3

[a]Thickness of the TiO_2 photoanode layer was approximately 1.2 μm.
[b]Heterostructured photoanode consisted of 400-nm-thick om-TiO_2 IF, 7-μm-thick nc-TiO_2, and 1.2-μm-thick om-TiO_2 BS as the bottom, middle, and top layers, respectively.

(H_2PtCl_6) were purchased from Sigma-Aldrich (St. Louis, MO). Tetrahydrofuran (THF), N-methyl pyrrolidone (NMP), methanol, 2-propanol, chloroform, acetonitrile, diethylether, and ethyl acetate were purchased from J.T. Baker. Deionized water (>18 MΩ·m) was obtained with a water purification system made by the Millipore Corporation. Ruthenium dye (535-bisTBA, N719) and TiO_2 colloidal paste (Ti-Nanoxide, D20) were purchased from Solaronix, Switzerland. Fluorine-doped tin oxide (FTO) conducting glass substrate (TEC8, 8 ohms/sq, 2.3 mm thick) was purchased from Pilkington, France. The purities of chemicals employed in this work were higher than 99%, and all chemicals were utilized without additional purification.

Synthesis of the two kinds of graft copolymer templates (PVC-*g*-POEM). The two kinds of graft copolymer templates were synthesized via an atomic transfer radical polymerization (ATRP) process according to our previously reported method[29]. In brief, PVC (6 g) was dissolved in 50 mL of NMP by stirring at 90°C for 4 h. After cooling the solution to room temperature, various amounts (9 g and 36 g) of POEM, 0.1 g of CuCl, and 0.23 mL of HMTETA were added to the solution. The green mixtures were stirred until homogeneous and then purged with nitrogen for 30 min. The reaction was carried out at 90°C for 18 h. After polymerization, resultant mixtures were diluted with THF. After passing the solutions through a column with activated Al_2O_3 to remove the catalyst, the solutions were precipitated into methanol. The graft copolymer templates were purified by dissolving THF and reprecipitating into methanol three times. Then, the graft copolymer templates were dried in a vacuum oven overnight at room temperature. By using different weight ratios of PVC : POEM, graft copolymer templates for different refractive index were obtained.

Preparation of the TiO_2 sol-gel solution using two kinds of graft copolymer templates. The TiO_2 sol-gel solution based on graft copolymer template was prepared via a previously reported simple sol-gel process using titanium isopropoxide (TTIP), THF, HCl solution, and deionized water at room temperature for 3 hours[23]. As a brief synthetic procedure, 0.05 g of two kinds of PVC-*g*-POEM graft copolymer templates (weight ratios of PVC : POEM were 1 : 6 and 1 : 1.5, referred to as type 1 and type 2) were first dissolved in 3 ml of THF. Separately, a titanium precursor containing sol was obtained by slowly adding concentrated HCl (0.15 ml, 37 wt. %) to TTIP (0.3 mL) under vigorous stirring. An additional 0.15 ml of DI water was slowly added to the TTIP solution. In this case, the volume ratio of [TTIP] : [HCl] : [H_2O] was 2 : 1 : 1. After aging for 15 min, the TTIP solution was slowly added to the PVC-*g*-POEM graft copolymer solution under stirring. This solution was subsequently aged under mild stirring at room temperature for 3 hours to prepare two kinds of om-TiO_2 layer structures.

Fabrication of om-TiO_2 BS layer based on photoanode. In a previous report, we showed that SiO_2 colloidal suspensions and TiO_2 sol-gel solution form a uniform and transparent om-TiO_2 BS layer by the spin coating method[23]. In the current experiment, two types of materials (high and low refractive index TiO_2 sol-gel solution) for om-TiO_2 BS were prepared separately. Before fabricating an om-TiO_2 BS layer, the FTO glasses were ultrasonically cleaned sequentially in isopropanol and chloroform for 30 min each and then dried in air. The om-TiO_2 BS multilayer structure was constructed by alternate deposition of a high refractive index om-TiO_2 structure based on type 1 (PVC-*g*-POEM graft copolymer with a high grafting degree) and low refractive index om-TiO_2 structure based on type 2 (PVC-*g*-POEM graft copolymer with a low grafting degree). These were deposited on as-prepared clean FTO glasses by spin coating at 1500 rpm. Between each layer deposition, heat treatment was performed in a furnace at 500°C for 1 hour to remove water bonded to the TiO_2 nanoparticle surfaces and mechanically stabilize the entire structure. The sequence of om-TiO_2 BS deposition was usually high refractive index om-TiO_2 layer, low refractive om-TiO_2 layer, high refractive index om-TiO_2 layer, and so on. Finally, om-TiO_2 BS was slowly heated at 450°C for 30 min under air conditions to decompose the graft copolymer templates and ensure interconnection between TiO_2 nanoparticles.

Dye adsorption of photoanode. To adsorb the dye molecules, the prepared photoelectrode based on om-TiO_2 BS layers were immersed into 10^{-4} M ruthenium dye (N719) solution in ethanol, and sensitized for one night at 50°C in a dark room. Afterward, this photoanode was rinsed with absolute ethanol in order to remove physisorbed ruthenium dye molecules.

Preparation of counter electrode. Transparent glasses coated with FTO glass were used for counter electrodes. The glasses were cleaned by sonication in isopropanol and then in chloroform. The counter electrodes were fabricated by thermal depositing H_2PtCl_6 solution (4 wt% in isopropanol) onto the conductive FTO glass followed by thermal sintering at 450°C for 30 min and cooling to 30°C over 8 h.

DSSC assembly using om-TiO_2 BS layers. Our previous method was used to fabricate solid PIL-based DSSCs with poly(1-((4 ethenylphenyl)methyl)-3-butyl-imidazolium iodide) (PEBII)[19,23,24]. The solid electrolyte solution deeply infiltrated into the photoanode and covered the counter electrode according to a previously reported procedure[30]. In brief, dilute PEBII electrolyte solution (2 wt. %) was first cast onto a photoanode based on om-TiO_2 BS and slowly evaporated for facile infiltration of electrolytes through the DSSCs. A dense PEBII electrolyte solution (10 wt. %) was then cast onto the photoanode to reduce the time required to evaporate solvent while preventing the formation of cavities between the two electrodes during solvent evaporation. Next, cells were placed in a drying oven at 40°C for 24 h to ensure complete solvent evaporation. The DSSCs were placed in a vacuum oven for one day to permit complete evaporation of the solvent and then sealed with an epoxy resin.

Materials characterization. Ellipsometric data (Thickness and refractive index) were taken on a spectroscopic ellipsometer (Alpha-SE) and the instrument software (Complete EASE software package, J.A. Woollam) was used to analyze the data. Field emission-scanning electron microscope (SUPRA 55VP, Carl Zeiss) was used to investigate the surface morphology and cross-section of the om-TiO_2 BS layers. The diffused reflectance spectra and absorption spectra were measured on a UV–visible spectrophotometer (Hewlett- Packard, Hayward, CF) to analyse the diffuse reflectance of films and dye amounts detached from films, respectively.

Solar cell characterization. The incident photo to current conversion efficiency (IPCE) spectra were measured with a spectral resolution of 5 nm using a 300 W xenon lamp and a monochromator equipped with order sorting filters (K3100). The IPCE value was calculated using the following equation 3.

$$IPCE = hcI/\lambda p \tag{3}$$

where *h* and *c* represent Planck's constant and the speed of light in a vacuum, respectively. *I* is the photocurrent density (mA/cm²). λ and P are the wavelength (nm) and the intensity (mA/cm²) of the incident monochromatic light, respectively. The EIS data were measured with a compactstat electrochemistry analyzer (IVIUM Technologies), with a frequency range from 0.01 Hz to 0.1 MHz and a potential modulation of 0.2 V under AM 1.5 (100 mW/cm²) light illumination. Current–voltage (*I–V*) characteristics of DSSCs were measured under an illumination (AM1.5, 1 Sun) using a Keithley Model 2400 (1000 W xenon lamp, Oriel, 91193). A typical cell had an active area of ca. 0.16 cm² and was masked using an aperture of the same area during the *I–V* measurements. A correction for the spectral mismatch between the simulated light and natural sunlight was made against a certified reference Si solar cell (Fraunhofer Institute for Solar Energy System, Mono-Si + KG filter, Certificate No. C-ISE269) for a sunlight intensity of one (100 mW/cm²). This calibration was verified with an NREL-calibrated Si solar cell (PV Measurements Inc.). The DSSCs temperature was maintained at 25°C throughout the measurement time using peltier cooling apparatus. The photoelectrochemical performances were calculated by the following equations.

$$FF = V_{max} \cdot J_{max} / V_{oc} \cdot J_{sc} \tag{4}$$

$$\eta(\%) = V_{max} \cdot J_{max} \cdot 100 / P_{in} = V_{oc} \cdot J_{sc} \cdot FF \cdot 100 / P_{in} \tag{5}$$

where J_{sc} is a short-circuit current density (mA/cm²), V_{oc} is an open-circuit voltage (V), P_{in} is an incident light power, *FF* is the fill factor, η is an overall energy conversion efficiency and J_{max} (mA/cm²) and V_{max} (V) are the current density and voltage in the *J-V* curve, respectively, at the point of maximum power output.

1. O'Regan, B. & Grätzel, M. A low-cost, high-efficiency solar cell based on dye-sensitized colloidal TiO_2 films. *Nature* **353**, 737–740 (1991).
2. Chatterjee, S., Patra, A. K., Bhaumik, A. & Nandi, A. K. Poly[3-(2-hydroxyethyl)-2,5-thienylene] grafted reduced graphene oxide: an efficient alternate material of TiO_2 in dye sensitized solar cells. *Chem. Commun.* **49**, 4646–4648 (2013).

3. Hosseini, T., Flores-Vivian, I., Sobolev, K. & Kouklin, N. Concrete Embedded Dye-Synthesized Photovoltaic Solar Cell. *Sci. Rep.* **3**, 2727; DOI:10.1038/srep02727 (2013).
4. Lv, M. *et al.* Optimized porous rutile TiO_2 nanorod arrays for enhancing the efficiency of dye-sensitized solar cells. *Energy Environ. Sci.* **6**, 1615–1622 (2013).
5. Huang, F. *et al.* Dual-function scattering layer of submicrometer-sized mesoporous TiO_2 beads for high-efficiency dye-sensitized solar cells. *Adv. Funct. Mater.* **20**, 1301–1305 (2010).
6. Xu, D., Zhang, H., Chena, X. & Yan, F. Imidazolium functionalized cobalt tris(bipyridyl) complex redox shuttles for high efficiency ionic liquid electrolyte dye-sensitized solar cells. *J. Mater. Chem. A* **1**, 11933–11941 (2013).
7. Chu, L. *et al.* Y. General Method for Preparing Anatase TiO_2 Treelike-Nanoarrays on Various Metal Wires for Fiber Dye-Sensitized Solar Cells. *Sci. Rep.* **4**, 4420; DOI:10.1038/srep04420 (2014).
8. Bella, F. *et al.* UV-crosslinked polymer electrolyte membrane for quasi-solid dye-sensitized solar cells with excellent efficiency and durability. *Phys. Chem. Chem. Phys.* **15**, 3706–3711 (2013).
9. Chan, Y.-F., Wang, C.-C. & Chen, C.-Y. Quasi-solid DSSC based on a gel-state electrolyte of PAN with 2-D graphenes incorporated. *J. Mater. Chem. A* **1**, 479-5486 (2013).
10. Yanagida, S., Yu, Y. & Manseki, K. Iodine/Iodide-Free dye-sensitized solar cells. *Acc. Chem. Res.* **42**, 1827–1838 (2009).
11. Jiang, K. J. *et al.* Photovoltaics based on hybridization of effective dye-sensitized titanium oxide and hole-conductive polymer P3HT. *Adv. Funct. Mater.* **19**, 2481–2485 (2009).
12. Johansson, E. M. J. *et al.* Combining a small hole-conductor molecule for efficient dye regeneration and a hole-conducting polymer in a solid-state dye-sensitized solar cell. *J. Phys. Chem. C* **116**, 18070–18078 (2012).
13. Yuan, W. *et al.* Synthesis and characterization of the hole-conducting silica/polymer nanocomposites and application in solid-state dye-sensitized solar cell. *ACS Appl. Mater. Interfaces* **5**, 4155–4161 (2013).
14. Li, Q. *et al.* High-temperature solid-state dye-sensitized solar cells based on organic ionic plastic crystal electrolytes. *Adv. Mater.* **24**, 945–950 (2012).
15. Tefashe, U. M. *et al.* Effect of cation on dye regeneration kinetics of N719-sensitized TiO_2 films in acetonitrile-based and ionic-liquid-based electrolytes investigated by scanning electrochemical microscopy. *J. Phys. Chem. C* **116**, 4316–4323 (2012).
16. Snaith, H. J. Perovskites: The Emergence of a New Era for Low-Cost, High Efficiency Solar Cells. *J. Phys. Chem. Lett.* **4**, 3623–3630 (2013).
17. Burschka, J. *et al.* Sequential deposition as a route to high-performance perovskite-sensitized solar cells. *Nature.* **499**, 316–319 (2013).
18. He, M. *et al.* High efficiency perovskite solar cells: from complex nanostructure to planar heterojunction. *J. Mater. Chem. A.* **2**, 5994–6003 (2014).
19. Park, J. T. *et al.* Hybrid templated synthesis of crack-free, organized mesoporous TiO_2 electrodes for high efficiency solid-state dye-sensitized solar cells. *Adv. Funct. Mater.* **23**, 26–33 (2013).
20. Colodrero, S. *et al.* Porous one-dimensional photonic crystals improve the power-conversion efficiency of dye-sensitized solar cells. *Adv. Mater.* **21**, 764–770 (2009).
21. Colodrero, S. *et al.* Efficient transparent thin dye solar cells based on highly porous 1D photonic crystals. *Adv. Func. Mater.* **22**, 1303–1310 (2012).
22. Colonna, D. *et al.* Introducing structural colour in DSCs by using photonic crystals: interplay between conversion efficiency and optical properties. *Energy Environ. Sci.* **5**, 8238–8243 (2012).
23. Park, J. T. *et al.* Enhancing the performance of solid-state dye-sensitized solar cells using a mesoporous interfacial titania layer with a Bragg Stack. *Adv. Func. Mater.* **23**, 2193–2200 (2013).
24. Park, J. T. *et al.* Bragg Stack-functionalized counter electrode for solid-state dye-sensitized solar cells. *ChemSusChem* **6**, 856–864 (2013).
25. Prosser, J. H. *et al.* Avoiding cracks in nanoparticle films. *Nano Lett.* **12**, 5287–5291 (2012).
26. Wu, Z., Lee, D., Rubner, M. F. & Cohen, R. E. Structural color in porous, superhydrophilic and self-cleaning SiO_2/TiO_2 Bragg Stacks. *Small* **3**, 1445–1451 (2007).
27. Calvo, M. E. *et al.* Photoconducting Bragg mirrors based on TiO_2 nanoparticle multilayers. *Adv. Funct. Mater.* **18**, 2708–2715 (2008).
28. Guldin, S. *et al.* Tunable mesoporous Bragg reflectors based on block-copolymer self-assembly. *Adv. Mater.* **23**, 3664–3668 (2011).
29. Ahn, S. H. *et al.* Direct assembly of preformed nanoparticles and graft copolymer for the fabrication of micrometer-thick, organized TiO_2 films: high efficiency solid-state dye-sensitized solar cells. *Adv. Mater.* **24**, 519–522 (2012).
30. Park, J. T., Koh, J. H., Seo, J. A. & Kim, J. H. Formation of mesoporous TiO_2 with large surface areas, interconnectivity and hierarchical pores for dye-sensitized solar cells. *J. Mater. Chem.* **21**, 17872–17880 (2011).
31. Sánchez-Sobrado, O., Calvo, M. E. & Míguez, H. Versatility and multifunctionality of highly reflecting Bragg mirrors based on nanoparticle multilayers. *J. Mater. Chem.* **20**, 8240–8246 (2010).
32. Kingery, W. D., Bowen, H. K. & Uhlmann, D. R. *Introduction to Ceramics* [669–677]. (New York, 1976).
33. Choi, S. Y. *et al.* Mesoporous Bragg stack color tunable sensors. *Nano Lett.* **6**, 2456–2461 (2006).
34. Park, J. T. *et al.* Facile fabrication of vertically aligned TiO_2 nanorods with high density and rutile/anatase phases on transparent conducting glasses: high efficiency dye-sensitized solar cells. *J. Mater. Chem.* **22**, 6131–6138 (2012).
35. Sauvage, F. *et al.* Effect of Sensitizer Adsorption Temperature on the Performance of Dye-Sensitized Solar Cells. *J. Am. Chem. Soc.* **133**, 9304–9310 (2011).
36. Bisquert, J. *et al.* Electron Lifetime in Dye-Sensitized Solar Cells: Theory and Interpretation of Measurements. *J. Phys. Chem. C* **113**, 17278–17290 (2009).
37. Park, J. T. *et al.* Preparation of TiO_2 spheres with hierarchical pores via grafting polymerization and sol-gel process for dye-sensitized solar cells. *J. Mater. Chem.* **20**, 8521–8530 (2010).

Acknowledgments

This work was supported by a National Research Foundation (NRF) grant and funded by the Korean government (MEST) through the Active Polymer Center for Pattern Integration (2007-0056091) and the Core Research Program (2012R1A2A2A02011268). D. L. acknowledges the support of NSF CBET-1234993 and NSF DMR-1055594.

Author contributions

J.T.P., D. L. and J.H.K. contributed to the conception and design of the experiment, analysis of the data and writing the manuscript with assistance of W.S.C. and S.J.K. J.T.P. carried out synthesis of materials, preparation of the devices, device performance measurements together with W.S.C. and S.J.K.

Additional information

Supplementary information accompanies this paper at http://www.nature.com/scientificreports

Competing financial interests: The authors declare no competing financial interests.

How to cite this article: Park, J.T., Chi, W.S., Kim, S.J., Lee, D. & Kim, J.H. Mesoporous TiO_2 Bragg Stack Templated by Graft Copolymer for Dye-sensitized Solar Cells. *Sci. Rep.* **4**, 5505; DOI:10.1038/srep05505 (2014).

This work is licensed under a Creative Commons Attribution-NonCommercial-NoDerivs 4.0 International License. The images or other third party material in this article are included in the article's Creative Commons license, unless indicated otherwise in the credit line; if the material is not included under the Creative Commons license, users will need to obtain permission from the license holder in order to reproduce the material. To view a copy of this license, visit http://creativecommons.org/licenses/by-nc-nd/4.0/